Journal of Power Sources 271 (2014) 334–341

Contents lists available at ScienceDirect

Journal of Power Sources

journal homepage: www.elsevier.com/locate/jpowsour

Improved lithium-metal/vanadium pentoxide polymer battery incorporating crosslinked ternary polymer electrolyte with N-butyl-N-methylpyrrolidinium bis(perfluoromethanesulfonyl)imide

Irene Osada [a], Jan von Zamory [a], Elie Paillard [a, *], Stefano Passerini [a, b, c, *]

[a] Institute of Physical Chemistry, University of Münster, Corrensstrasse 28/30, 48149 Münster, Germany
[b] Helmholtz Institute Ulm, Electrochemical Energy Storage, Albert-Einstein-Allee 11, 89081 Ulm, Germany
[c] Karlsruher Institute of Technology (KIT), PO Box 3640, 76021 Karlsruhe, Germany

HIGHLIGHTS

- Li-metal/V_2O_5 polymer batteries using crosslinked polymer electrolyte were prepared and tested.
- The partial formation of the ω-phase is beneficial for battery performance.
- The specific energy vs. Li metal per weight of V_2O_5 is as high as 796 Wh kg^{-1}.
- After 200 cycles at 40 °C and C/10, the specific energy is still above 660 Wh kg^{-1}.

ARTICLE INFO

Article history:
Received 14 April 2014
Received in revised form
29 July 2014
Accepted 3 August 2014
Available online 12 August 2014

Keywords:
V_2O_5
Solid polymer electrolyte
Lithium polymer battery
PEO
Ionic liquid
TFSI

ABSTRACT

Li metal polymer batteries incorporating crosslinked ternary PEO/PYR_{14}TFSI/LiTFSI solid polymer electrolyte (SPE) have been prepared, using V_2O_5 as active cathode material. As a result of the optimization of the SPE as well as the cell assembly and cycling conditions, V_2O_5 lithium metal polymer batteries allow reaching 796 Wh kg^{-1} (of V_2O_5) at C/10 at 40 °C and maintaining 663 Wh kg^{-1} after 200 cycles at 40 °C. This is higher than the theoretical specific energy of $LiCoO_2$ vs. Li of 609 Wh kg^{-1}. Cycling at 80 °C allows reaching 270 mAh g^{-1} at C/2 and 210 mAh g^{-1} at 1 C, while at 20 °C it is still possible to reach a discharge capacity of almost 100 mAh g^{-1} at low rates. Post-cycling SEM and EDX imaging showed that, after 200 cycles at 40 °C, if the plating of Li is not fully homogeneous, no sign of dendrite growth nor obvious vanadium dissolution and redeposition on the anode side occurred.

1. Introduction

These recent years have seen the fast development of electric (and hybrid) cars, driven by the ecological awareness as well as fear of increasing oil-prices in the long term. The driving ranges of fully electric cars from 80 to 480 km are already far above the average commuting distance in most countries. However, they are seen as a main limitation to their commercial breakthrough, which leads to the need for higher energy density EV batteries. In addition, recent incidents showed that the mere upscaling of the current Li-ion battery technology bears severe safety risks.

So far, the market is dominated by Li-ion batteries, whose technology is directly derived from those used in portable electronics. That is an insertion carbonaceous anode with a capacity below 372 mAh g^{-1}, and an electrolyte made of ethylene carbonate (EC) [1,2] mixed with linear alkyl carbonates, such as dimethyl carbonate (DMC), diethyl carbonate (DEC) and ethyl methyl carbonate (EMC), for lowering the viscosity and melting points of solvent mixtures. These solvents present serious safety risks due to their high volatility and low flash points ($T_{F(DMC)}$ = 17 °C; $T_{F(DEC)}$ = 25 °C; $T_{F(EMC)}$ = 23 °C). Moreover, the electrolytes include $LiPF_6$, as it inhibits Al corrosion [3–10]. Unfortunately, PF_6^- is extremely sensitive to hydrolysis [3,11] and leads to HF formation in presence of water traces above 60 °C, in addition to its intrinsic low

* Corresponding authors. Institute of Physical Chemistry, University of Münster, Corrensstrasse 28/30, 48149 Münster, Germany.
E-mail addresses: Elie.Paillard@uni-muenster.de (E. Paillard), Stefano.passerini@kit.edu (S. Passerini).

http://dx.doi.org/10.1016/j.jpowsour.2014.08.019
0378-7753/

thermal and chemical stability [12,13]. Thus, the operation of Li-ion batteries is limited to temperatures below 55 °C, even lower for reasonable aging. Indeed, the ageing of Li-ion batteries is strongly related to the parasitic reactions at the anode/electrolyte interface [14], which are accelerated at elevated temperature [15]. Moreover, at elevated temperatures, the direct reaction with the electrolyte generates heat [16–19] which can contribute to the thermal runaway, leading to oxygen generation at the cathode and electrolyte combustion [20]. Thus, high capacity EV Li-ion batteries based on conventional electrolytes need cooling during operation, which in turn consumes part of the stored energy and limits the driving range.

On the other hand, Li-metal polymer batteries are used in commercial electric cars since 2011 with performances in line with Li-ion batteries powered cars that is 250 km driving range for Bollore's BlueCar. These secondary batteries include a Li metal anode offering a capacity of 3860 mAh g^{-1}. Even though, this electrode never met commercial success with liquid electrolytes, despite early reports [21]. The use of PEO-based solid polymer electrolytes (SPEs) enables the use of elemental lithium despite its high reactivity, similarly to graphite, through the formation of a favorable Solid Electrolyte Interphase (SEI) [22,23] at its interface with the electrolyte. One major advantage of SPEs, in addition to their favorable interfacial properties with Li metal, is their high thermal stability and low volatility. However, the main drawback of Li-metal polymer batteries remains their low temperature performance. Indeed, PEO-based electrolytes are reasonably conductive (5×10^{-4}–10^{-3} S cm^{-1}) only above 70°–80 °C, even if their low temperature performance can be improved by decreasing their crystallinity, for instance by cross-linking [24–26] or use of PPO/PEO copolymers [27,28]. Even though plasticizers have been proposed for improving SPE low temperature performance [29,30], the use of molecular additives leads to the same volatility issues as for liquid or gel electrolytes. Thus, the use of ionic liquids (ILs) as non-volatile and non-flammable co-solvents has been proposed, enabling Li-metal battery operation at 40 °C [31–34]. Contrary to alkyl carbonates, which are not known to be favorable for Li homogeneous deposition, IL-based electrolytes have been reported to allow good performance of the Li metal electrode [35,36].

Since the first report on ternary PEO/IL/Li salt SPEs, progresses have been made in their preparation by crosslinking, which ensures extended amorphous domains, even after long resting periods [37] and improved performances [38,39]. In addition, in a system heavily plasticized, crosslinking allows obtaining dimensional stability, combined with beneficial elastomeric properties, contrary to (liquid electrolyte + separator) ensembles which cannot accommodate the volume changes of the Li anode. Finally, the excellent stability of $TFSI^{-}$[1] based ILs allows direct crosslinking of the ternary SPE precursor paste in a solvent free processing.

Recently, excellent performance was reported using $LiFePO_4$ as a cathode material [40,41] in Li-metal polymer cells incorporating crosslinked ternary PEO/N-butyl-N-methyl pyrrolidinium bis(trifluoromethanesulfonyl)imide ($PYR_{14}TFSI$)/LiTFSI electrolyte. However, the performance of high voltage oxides such as $LiNi_{0.8}Co_{0.8}Al_{0.05}O_2$ and $LiNi_{0.33}Mn_{0.33}Co_{0.33}O_2$ show severe decays, given their high operating potentials which are not compatible with PEO-based anodic stability in contact with particulate electrodes [42,43].

Thus, one way of improving the energy density of Li-metal batteries is using lower operation potentials active materials with high capacities, which increases the overall stability and lifetime of the system. One of the well known candidates for this are the vanadium oxides, among which layered V_2O_5 [44–46] is now experiencing a renascence giving the possibility of inserting up to three Li^+ per formula unit [46,47].

This material had previously been reported in Li-metal polymer batteries incorporating non-crosslinked ternary SPE [33,48–50]. The performances of such batteries are reported in Table 1 together with the results of cross-linked SPE in Li/$LiFePO_4$ batteries. With V_2O_5, capacities up to 210 mAh g^{-1} were formerly reached, resulting despite its lower operating voltage, in energy densities up to 588 Wh kg^{-1}. However, a 40% capacity decay occurred within 80 cycles. On the other hand, $LiFePO_4$, despite its higher operating voltage, led to lower specific energy, but was able to maintain its performance for more than 200 cycles.

Here we report on the optimization of Li/ternary polymer electrolyte/V_2O_5 battery by the use of cross-linked ternary SPE as well the tuning of the cycling conditions and the cell preparation, with the target of reaching both high energy densities and extended cycle life. The effect of temperature was assessed in the 20 °C - 80 °C range and the morphology of the Li electrode after 200 cycles was investigated.

2. Experimental section

2.1. Synthesis of N-butyl-N-methylpyrrolidinium bis(trifluoromethanesulfonyl)imide and bis(fluorosulfonyl)imide ($PYR_{14}TFSI$)

$PYR_{14}TFSI$ and $PYR_{14}FSI$ were synthesized according to an already reported procedure [51–53] using N-methylpyrrolidine (97 wt%, Aldrich), 1-bromobutane (99 wt%, Aldrich), ethylacetate (ACS grade > 99.5 wt%, Aldrich) and LiTFSI (3 M) or KFSI (Suzhou Fluolyte) as received. The purity of the ILs was checked by ^1H NMR and ^{13}C NMR for organic impurities and by ICP-OES for halide contaminants. The water content, after drying at 100 °C and 10^{-7} mbar for 24 h was below 3 ppm as determined by Karl-Fischer coulometric titration (Mettler Toledo).

2.2. Preparation of the cross-linked SPE and the composite cathode tape

The ternary SPEs were prepared according to reference [38]. The SPE was prepared by mixing poly(ethylenoxide) (PEO) (Dow Chemical, M_W = 4.000.000), $PYR_{14}TFSI$, and LiTFSI (3 M, dried at

Table 1
Specific capacity and discharge energy reported for Li-metal polymer batteries including V_2O_5 or $LiFePO_4$.

	Discharge capacity[b]/mAh g^{-1}	Specific discharge energy[b,c]/Wh kg^{-1}
V_2O_5 [33] (2.0–3.6 V)		
20 °C	24 (C/20)	62
	44 (C/20)[a]	114
30 °C	61 (C/20)	159
	95 (C/20)[a]	247
40 °C	210 (C/20) (2nd cycle)	588
	150 (C/20) (50th cycle)	390
	125 (C/20) (80th cycle)	300
$LiFePO_4$ [40] (2.0–4.0 V)		
20 °C	114 (C/20)	390
40 °C	170 (C/20)	580
	168 (C/10)	575
	161 (C/5)	550

[a] Charge at C/50.
[b] Refers to active material weight.
[c] V estimated from graph, rounded up.

[1] $TFSI^{-}$ refers to the historical and most used term for this anion: Bis(trifluoromethanesulfonyl)imide. Its IUPAC name is $TFSA^{-}$ for bis(trifluoromethanesulfonyl)amide.

120 °C for 24 h under vacuum) in a (20:2:4) (EO/LiTFSI/$PYR_{14}TFSI$) molar ratio with benzophenone (5 wt%, Aldrich). After mixing, annealing and hot-pressing the SPE was crosslinked via UV radiation in a UV chamber (UVA Cube 100, Hönle) for 10 min.

The composite cathode was prepared as previously reported [33,38,40]. In a dry-room (H_2O < 20 ppm), V_2O_5 (Pechiney) and Ketjen black (KJB, Akzo Nobel) were dried at 110 °C under vacuum for 24 h and then dry mixed in a mortar. PEO and LiTFSI were dried under vacuum for 24 h at 50 °C and 120 °C respectively. The powder mixture was then blended with a paste-like mixture of PEO, LiTFSI and $PYR_{14}TFSI$ to reach the final weight ratio of 43.0/7.0/17.5/5.0/27.5 (V_2O_5/KJB/PEO/LiTFSI/$PYR_{14}TFSI$). The gum-like mixture was then annealed at 100 °C over night under vacuum and hot-pressed into films of a thickness of ca. 150 μm. The films were then calendered at room temperature to a thickness of 20–40 μm.

2.3. Li-metal batteries assembly

Li/polymer electrolyte/V_2O_5 cells were assembled in two electrodes vacuum sealed coffee-bag cells in a dry-room (H_2O < 20 ppm) by stacking the 50 μm Li foil (Rockwood Lithium), SPE, and cathode tape (Ø = 12 mm). The active mass loading of V_2O_5 was 2.7 ± 0.2 mg cm^{-2}. As current collectors, nickel and carbon-coated aluminum foils were used for, respectively, the anode and cathode. The cells were finally laminated at 100 °C before the electrochemical tests.

2.4. Electrochemical tests

The contact resistance between the composite cathode tape and two types of current collectors was measured using symmetrical Al/SPE/Al coffee bag cells, using either pristine Al or carbon coated Al, with a Solartron 1260 connected to a Solartron 1287 in the [100 kHz–1 Hz] range.

The cycling performance of Li/polymer electrolyte/V_2O_5 cells was evaluated with a battery cycler (S4000, Maccor Inc.). To control the cell temperature, climatic chambers (Binder, MK53) were used.

2.5. Thermal characterization

Differential scanning calorimetry (DSC) traces of composite cathode material have been recorded in order to investigate the cathode crystallinity as well as its thermal stability. The measurements were done using a TA Instrument Q2000. The samples were placed in aluminum pans hermetically sealed in a dry-room (H_2O < 20 ppm). The scans were performed at 5 °C min^{-1} for both cooling and heating, in He atmosphere. Reported T_g were measured at the inflexion point.

2.6. Morphological characterization

For SEM imaging and EDX mapping a Zeiss Auriga microscope was employed. The samples were prepared in the dry-room (H_2O < 20 ppm) and transferred to the SEM in under vacuum.

3. Results and discussion

3.1. Cathode characterization

3.1.1. Morphological characterization

The pristine V_2O_5 material is composed of particles of 200–500 nm in size, which form agglomerates with a size of ca. 40 μm, as it can be seen in Fig. 1.

The cathode tape was obtained under the form of a self-standing film as shown in Fig. 2a, exhibiting elastomeric properties, needed for buffering the volume changes and maintaining good interfacial contact during cycling. An SEM image of the cathode tape cross section, obtained after breaking the cathode tape quickly after cooling it in liquid N_2, is shown in Fig. 2b. It is obvious that the agglomerates are dispersed upon cathode preparation and that the primary particles are homogeneously dispersed, ensuring a good V_2O_5/electrolyte contact.

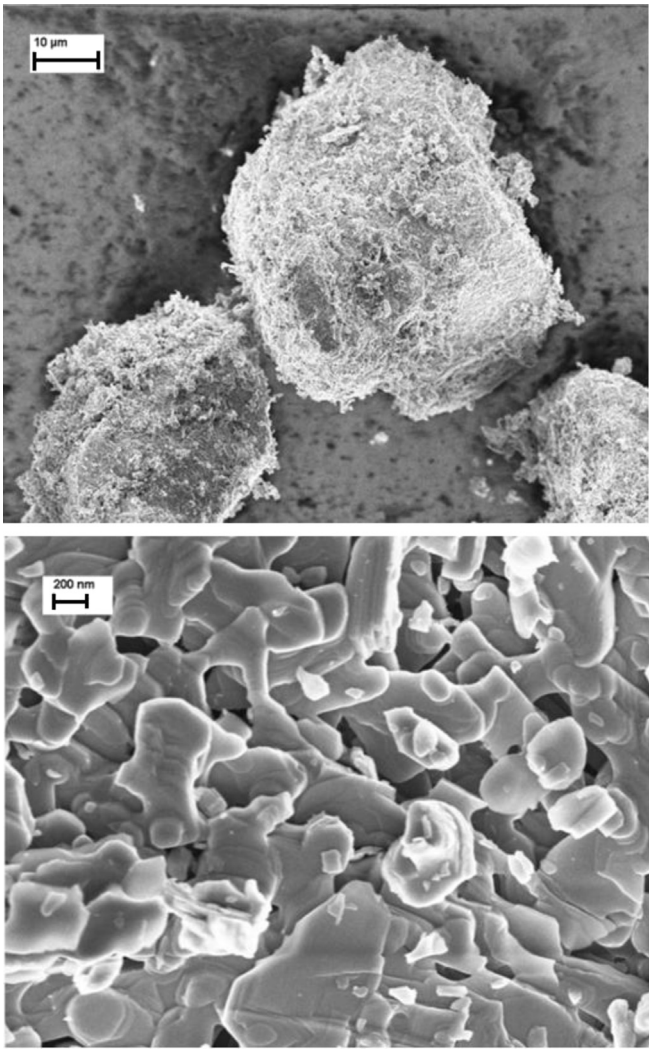

Fig. 1. SEM images of the pristine V_2O_5 material.

3.1.2. Thermal characterization

Three consecutive DSC heating ramps of the cathode tape are shown in Fig. 3. A T_g can be seen in all DSC traces, showing that the electrolyte is mostly amorphous. Although all scans showed melting peaks between 0 and 50 °C, the fusion enthalpies were comprised between 4.2 J g^{-1} and 5.5 J g^{-1} (related to weight of cathode). The comparison with the 100% crystalline PEO fusion enthalpy of 196.6 J g^{-1} [54] shows that ca. 5.0–6.5% of the PEO is crystalline in the composite cathode in the absence of crosslinking. Additionally, the first scan reveals a two-step melting, probably corresponding to the melting of the (2/1) $PYR_{14}TFSI$/LiTFSI [53] crystalline phase between 0 °C and 25 °C, followed by the melting of crystalline PEO. Interestingly, no degradation was observed up to 100 °C. In the following scans, a cold crystallization starts at c.a. −25 °C, directly followed by a wide melting peak. During the second scan, the T_g increases from −75 °C to −66 °C, probably as a result of an increased

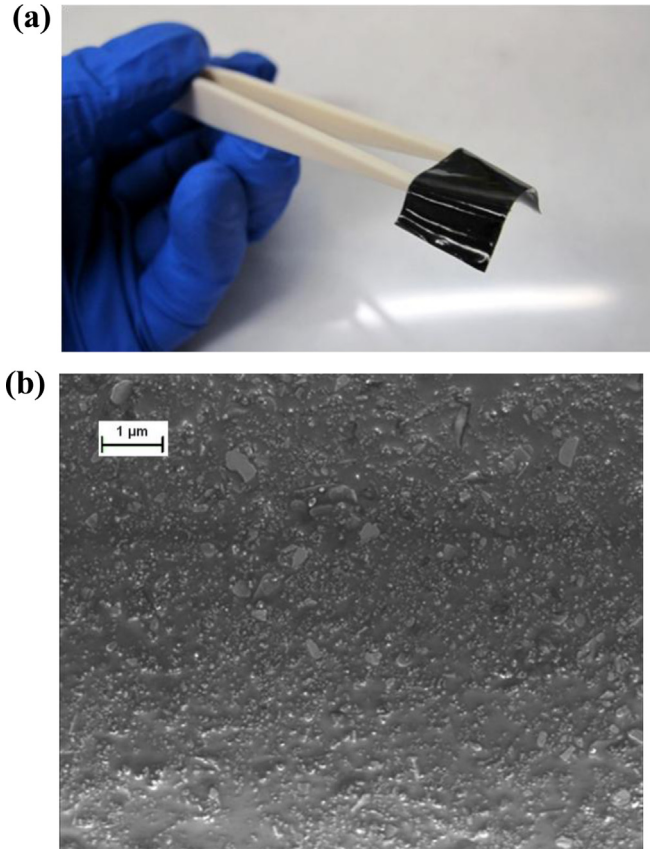

Fig. 2. (a): SEM image of the cathode tape. (b): SEM image of a cross section of the composite cathode tape.

Li content in the amorphous ternary phase. In addition, a limited exothermic process starts around 140 °C (i.e. similarly to PEO stability in O_2 [37]), possibly linked to reactions between PEO and V_2O_5 [43] or carbon additive surface groups. Despite this reactivity, the 3rd scan is similar to the second, with, however, no obvious exothermic reactions below 180–190 °C. Thus, even if minor surface reactions take place at the particle/electrolyte interface during the second scan, the system does not seem significantly modified (nor generates gas) up to ca. 200 °C.

3.2. Effect of the carbon coating on the current collector/cathode interfacial impedance

In the case of polymer self-standing cathodes, the presence of the SPE within the cathode can insulate the electronically conductive network formed within the electrode by the conductive additive (KJB) from the current collector. This might parent the establishment of a good contact at the interface with the current collector. Fig. 4 shows the impedance data of symmetrical Al/V_2O_5 cathode/Al cells immediately after assembly and after 30 days rest, for both pristine and carbon coated Al current collectors.

It is obvious that the resistance of the cell with the coated current collectors is much lower (four orders of magniture) than that including the pristine Al foil, due to the interpenetration of the thin particulate carbon coating and the composite cathode. It should be pointed out that other surface treatments could also modify the Al surface, both in terms of Al_2O_3 layer thickness and rugosity, although we chose a pristine Al foil as reference here. In the following, all current collectors used are C-coated.

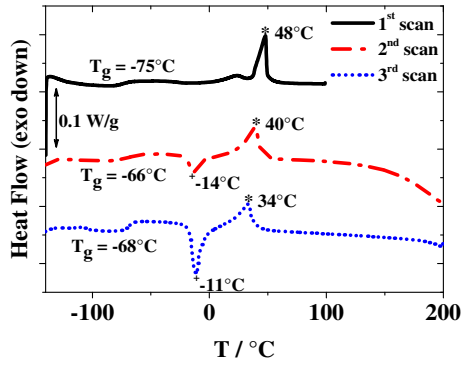

Fig. 3. DSC traces at 5 °C min^{-1} of V_2O_5 composite cathode in N_2.

3.3. Li/V_2O_5 polymer cells electrochemical behavior

3.3.1. Effect of temperature

Li/V_2O_5 cells have been galvanostatically cycled at temperatures ranging from 20 °C to 80 °C in the 2.0–4.0 V range with a 20 h 30 min time limit for each step, for limiting the Li insertion to slightly more than two Li^+ at low rate. The voltage profiles during the first discharge/charge cycle are shown in Fig. 5. At C/20, for temperatures above 20 °C, the plateaus corresponding to the successive phase changes from α to ω [46] are well defined, as shown in the graph. It is worth noticing that, for all temperatures above 20 °C, a small fraction of ω phase ($Li_xV_2O_5$, $x > 2$) is clearly formed at C/20, this last phase change being known to be irreversible [46].

As a result of the time limit, recharge efficiencies of 100% are obtained for all temperatures above 20 °C. It can be seen that the end of charge voltages decrease with temperature as a result of the extraction of the last Li^+ in the lattice being more sensitive to temperature. At 20 °C a capacity of 96 mAh g^{-1} is reached during the first discharge. However, the conductivity of the electrolyte is too low at this temperature for observing well defined plateaus.

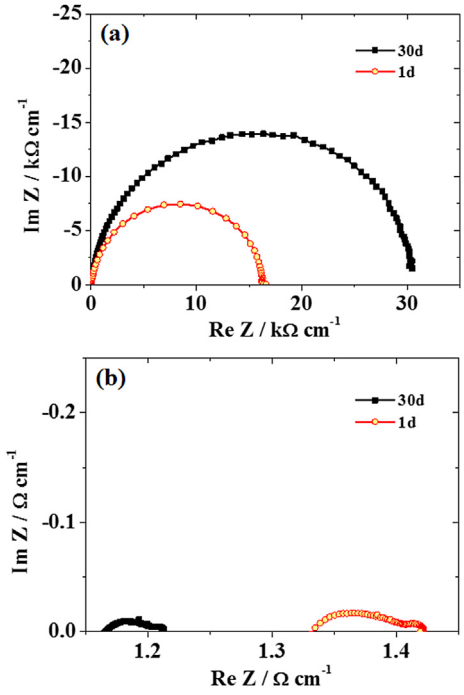

Fig. 4. Nyquist plot of an Al/V_2O_5 cathode/Al cell, after cell assembly and after 30d, at 20 °C. (a): uncoated Al, (b): carbon coated Al.

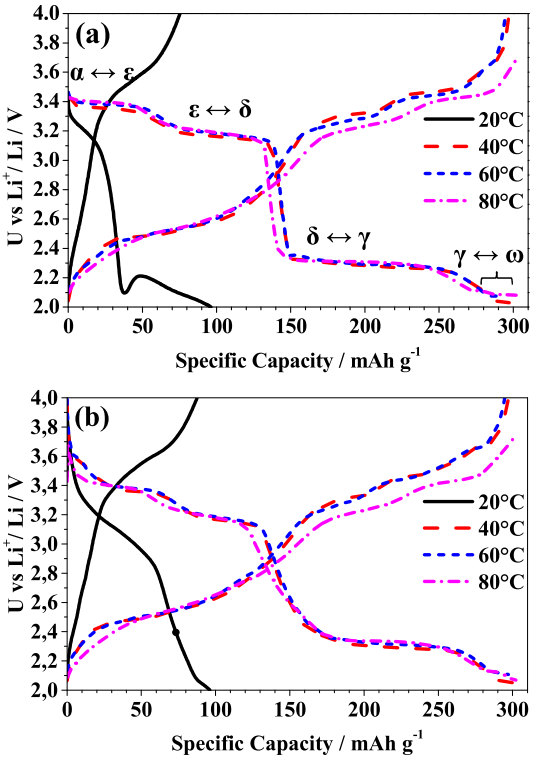

Fig. 5. Discharge/charge cycles at C/20, at different temperatures as indicated on the graph. 1 C = 295 mAh g^{-1} (a) 1st cycle (b) 2nd cycle.

Interestingly, when 2.1 V is reached, the cell voltage increases, reflecting an increase in electronic conductivity probably linked to the formation of a small fraction of ω phase, already at 20 °C. In the subsequent charge a coulombic efficiency of 78.3% is obtained. The superior performance of the cross-linked SPE is well evidenced by the comparison of the discharge capacities in Fig. 6 and those in Table 1 obtained with a non cross-linked SPE [33]. However, for reaching higher performance at low temperature, the use of a lower viscosity ionic liquid would be required, providing that the resulting electrolyte is amorphous and allows forming a proper SEI onto Li metal.

At 40 °C, 60 °C and 80 °C, the discharge plateaus are shifted to higher potentials during the second discharge and some additional capacity is delivered above 3.5 V, especially for the cells charged above 3.7 V in the first cycle (i.e. at 40 °C and 60 °C).

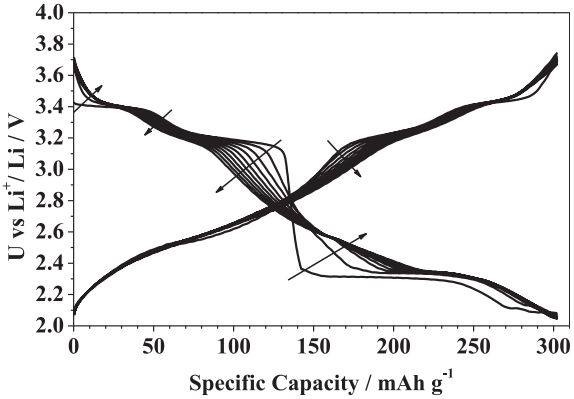

Fig. 6. Evolution of the voltage profile at 80 °C and C/20 during the first 10 cycles (1 C = 295 mAh g^{-1}).

The evolution of the voltage profiles at C/20 and 80 °C is illustrated in Fig. 6. It reveals that upon continuous cycling the voltage plateaus shorten. An increasing fraction of the delivered capacity is linked to the presence of the increasing fraction of the ω phase. This progressive conversion is rather neutral in terms of discharge voltage and is beneficial for the charge, thus increasing the overall energy efficiency of the cell.

The rate performance up to 5 C was tested between 20 °C and 80 °C and is summarized in Fig. 7a. The capacities at C/20 are fixed by the time limit, as mentioned earlier, which results in capacities of ca. 300 mAh g^{-1} above 20 °C. Starting from C/10, the performance of the cells strongly depends on the temperature. At 80 °C, capacities higher than 310 mAh g^{-1} are obtained at C/10 and C/5 and at 1 C the capacity delivered is still higher than

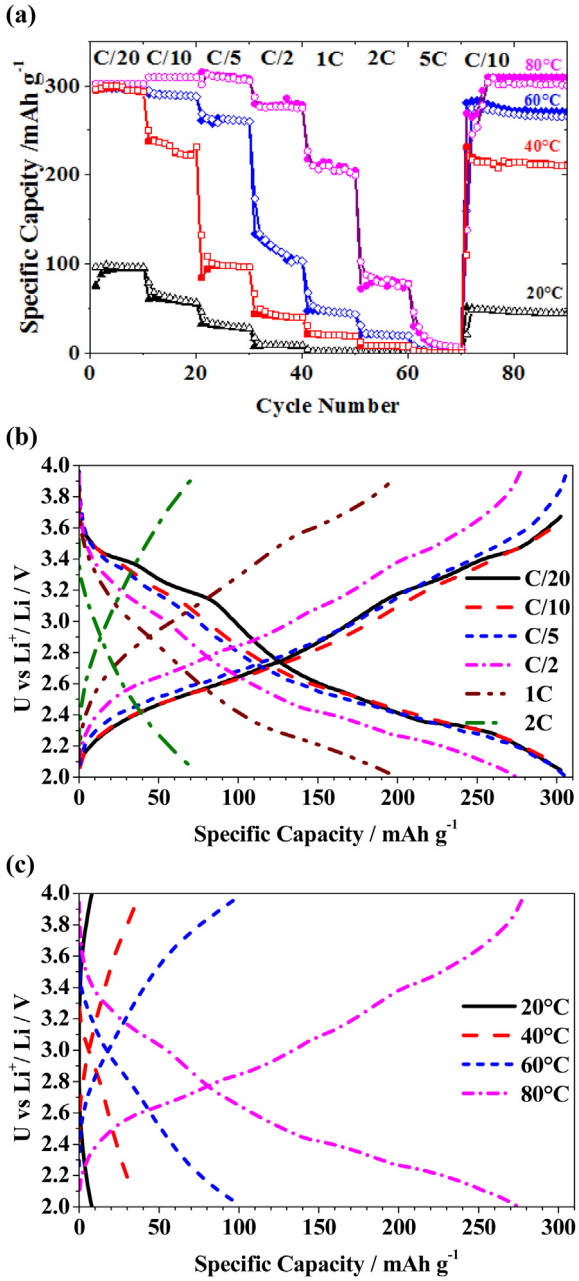

Fig. 7. (a) Rate capability of Li/V_2O_5 cells at various temperatures. Open symbols: charge. Filled symbols: discharge (b) Voltage profiles for the 10th, 20th, 30th, 40th, 50th and 60th cycles at 80 °C. (c) Comparison of voltage profiles at C/2 (40th cycles).

200 mAh g^{-1}. At 5 C, however, the electrolyte is not conductive enough at any temperature to allow delivering significant capacity. The voltage profiles at 80 °C (Fig. 7b) show that, even if some progressive conversion to the ω phase occurs, the successive reversible phase changes (α ↔ γ) are still visible after 50 cycles (at 1 C). The voltage profiles at C/2 are given in Fig. 7c for all tested temperatures. It is clear that, if the battery can deliver considerable capacities at low temperatures and moderate rates, 80 °C remains the temperature of choice when higher power is needed.

3.3.2. *Effect of cycling conditions on battery performance*

For assessing the beneficial effect of the presence of a limited amount of ω phase, the influence of formation cycles was investigated. Fig. 8 compares the performance at 40 °C of a cell cycled at C/20 for two cycles and then at C/10 to another cell cycled at C/10 since the first cycle. It is clear that the formation of the ω phase takes place more significantly at C/20 and that, in the following cycles, the voltage profile becomes slopier, indicating more conversion to the ω phase. More importantly, the charge plateaus are shifted toward lower voltages, while the discharge plateaus are shifted to higher voltages, which results in a neat capacity and energy efficiency improvement. One can also notice that a cut-off voltage higher than 3.7 V is required to charge the cathode which could also explain the lower capacities reported in previous work (see Table 1).

As a comparison, Fig. 9 shows the voltage profiles of a cell subjected to two cycles at C/20 then C/10 in the 2.0–3.7 V range, showing that only ca. 200 mAh g^{-1} can be cycled in these conditions. Nevertheless, the improvement of the SPE and cell preparation results in enhanced cycling stability and rate performance with less than 14% capacity fading in 100 cycles (from cycle 2) compared with >37% in previous reports [33].

Fig. 10 shows the long term cycling behavior at C/10 of a cell subjected to two formation cycles at C/20 at 40 °C and cycled in the 2.0–4.0 V range. One can notice that the mean voltages during cycling are rather constant (2.72–2.77 V for discharge). As a result, a specific discharge energy above 796 Wh kg^{-1} is obtained at C/10 in the 3rd cycle (834 Wh kg^{-1} at C/20 in the 1st cycle), which decreases to 663 Wh kg^{-1} after 200 cycles). Even with a lower operating voltage, the specific energy is higher than for a Li/$LiFePO_4$ polymer battery, although the capacity decay remains more pronounced with 16.5% loss in 200 cycles (from cycle 3).

It is possible to insert more Li^+ in the material and achieve the full conversion to the ω phase in the first cycle. Nevertheless, preserving most of the material morphology and using the ω phase

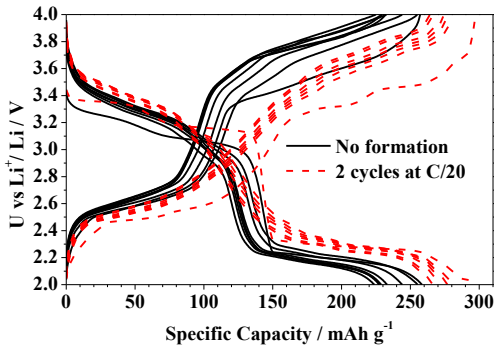

Fig. 8. Comparison between two cells cycled at C/10 including one cycled at C/20 for the two first cycles. The 1st, 10th, 20th, 30th, 40th, 50th, 60th and 70th cycle are shown (1 C = 295 mAh g^{-1}).

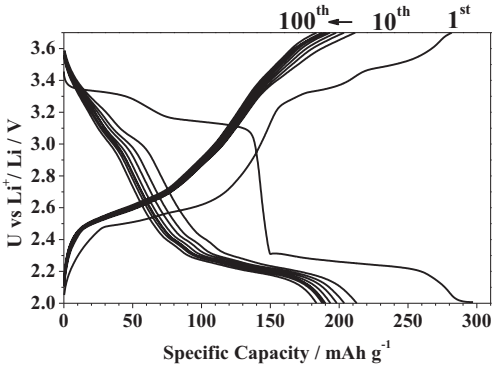

Fig. 9. Voltage profile of a Li/V_2O_5 cell at 40 °C. Cut-off voltages: 2.0–3.7 V. Current applied: two cycles at C/20, then C/10. The 1st, 10th, 20th, 30th, 40th, 50th, 60th, 70th, 80th, 90th, 100th cycle are shown.

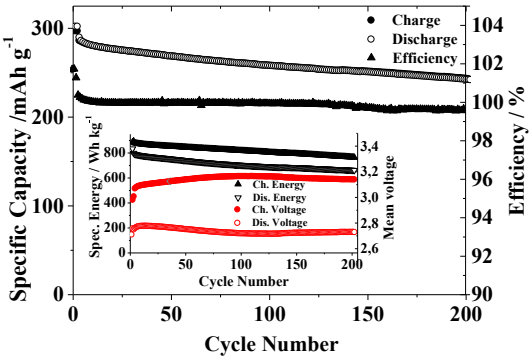

Fig. 10. Specific capacity and coulombic efficiencies of a Li/V_2O_5 polymer cell at 40 °C. First two cycles at C/20, then at C/10 (1 C = 295 mAh g^{-1}). Insert: mean voltage and specific energy.

only as a conductive doping phase results in higher energy densities, due to higher average discharge voltage. Fig. 11 shows the effect on the cell performance of setting 1.5 V as the lower cut-off voltage. Even though a first discharge capacity of 430 mAh g^{-1} is delivered, only around two equivalents of lithium can then be reversibly cycled into this phase and capacities around 300 mAh g^{-1} are reached also in this case. However, the average voltage decreases to values below 2.55 V and the specific energy is lower (excepted for the first discharge) with values around 720–725 Wh kg^{-1}.

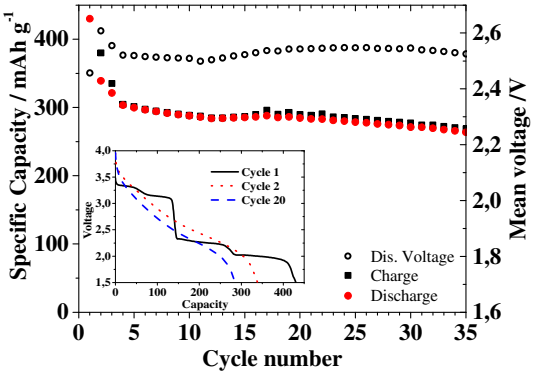

Fig. 11. Specific capacity and average discharge voltage of a Li/V_2O_5 polymer cell at 40 °C. First two cycles at C/50, then C/30 (1 C = 450 mAh g^{-1}). Cut-off voltages: 1.5–4 V.

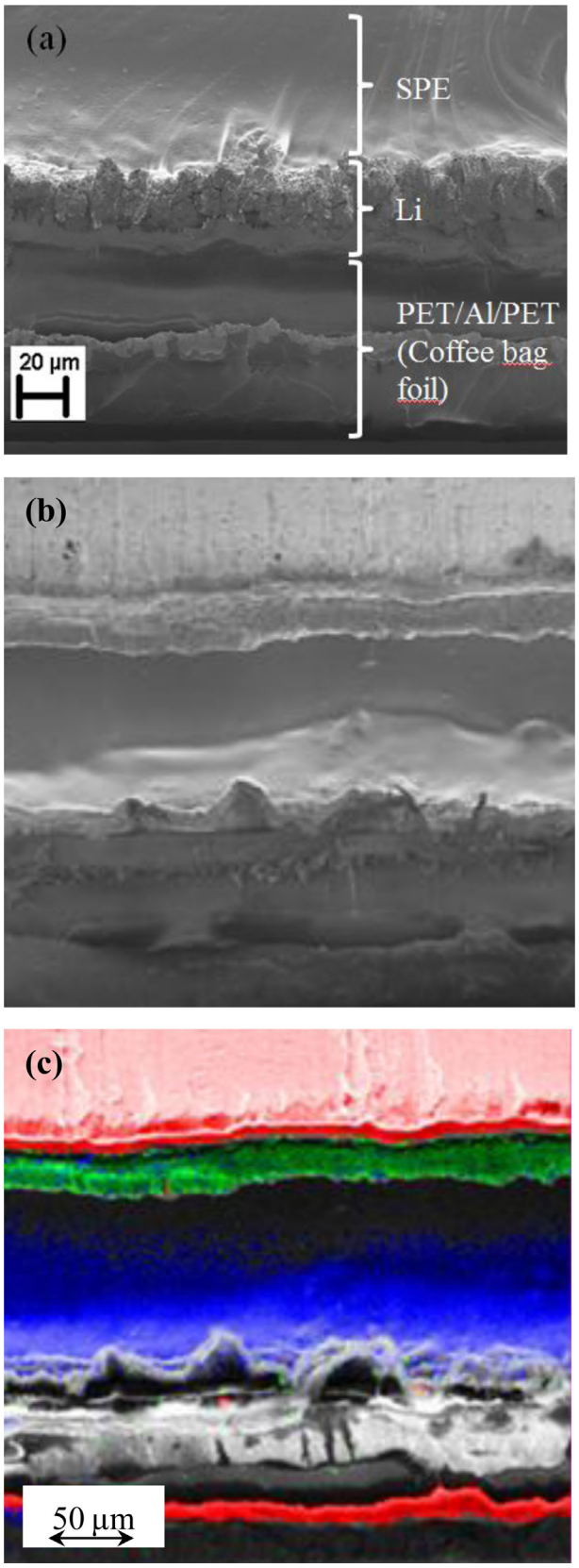

Fig. 12. (a) and (b): SEM images of the cross-section of a Li/V_2O_5 cell cycled for 200 cycles at C/10. (c): EDX mapping of the cross-section shown in (b): red: Al, green: V, blue: S. (For interpretation of the references to color in this figure legend, the reader is referred to the web version of this article.)

3.3.3. Post-cycling analysis of the battery after 200 cycles

The cell, whose electrochemical performance is reported in Fig. 10, has been cross-sectioned after dipping it in liquid N_2 in a dry-room. The SEM image of the cross-section is shown in Fig. 12a. It is obvious that the Li which has been cycled forms a less homogeneous layer on top of the original foil. Nevertheless, no sign of dendrites is seen in any part of the cross section. EDX analysis has been performed on a smaller area (c.f. Fig. 12a–b) and reveals no obvious vanadium dissolution and deposition on the Li anode despites few spots corresponding to vanadium, most likely due to the cutting of the cell.

4. Conclusion

Li/V_2O_5 polymer batteries able to deliver 796 Wh kg^{-1} (of V_2O_5) at 40 °C and C/10 were prepared, thanks to the use of cross-linked SPE, optimized cycling conditions and cell preparation. 663 Wh kg^{-1} were still delivered after 200 cycles at 40 °C. The batteries showed improved versatility in terms of temperature conditions, as they were able to deliver 270 mAh g^{-1} at C/2 at 80 °C and 95 mAh g^{-1} at 20 °C and C/20. The irreversible formation of a small fraction of ω phase was shown to have a beneficial effect on the performance of the cells, due to its favorable transport properties for Li^+ and e^-. However, the full conversion of the material results in a decreased specific energy, as compared to the case where this phase is used as an active dopant.

Acknowledgment

This work was supported by the European Commission within the FP7 Project LABOHR (FP7-2010-GC-Electrochemical-Storage 265971). Rockwood Lithium is acknowledged for providing the Li foil. We are grateful to G. B. Appetecchi (ENEA, Italy) for providing the V_2O_5 powder.

References

[1] R. Fong, U. von Sacken, J.R. Dahn, J. Electrochem. Soc. 137 (1990) 2009–2013.
[2] J.M. Tarascon, D. Guyomard, Solid State Ionics 69 (1994) 293–305.
[3] H. Yang, G.V. Zhuang, P.N. Ross Jr., J. Power Sources 161 (2006) 573–579.
[4] T. Nakajima, M. Mori, V. Gupta, Y. Ohzawa, H. Iwata, Solid State Sci. 4 (2002) 1385–1394.
[5] M. Morita, T. Shibata, N. Yoshimoto, M. Ishikawa, Electrochim. Acta 47 (2002) 2787–2793.
[6] S.S. Zhang, T.R. Jow, J. Power Sources 109 (2002) 458–464.
[7] H.S. Choe, B.G. Carroll, D.M. Pasquariello, K.M. Abraham, Chem. Mater. 9 (1997) 369–379.
[8] C. Iwakura, Y. Fukumoto, H. Inoue, S. Ohashi, S. Kobayashi, H. Tada, M. Abe, J. Power Sources 68 (1997) 301–303.
[9] K. Kanamura, T. Okagawa, Z.-i. Takehara, J. Power Sources 57 (1995) 119–123.
[10] X. Zhang, T.M. Devine, J. Electrochem. Soc. 153 (2006) B344–B351.
[11] C.G. Borlowz, Electrochem. Solid State Lett. 2 (1999) 362.
[12] C.L. Campion, W. Li, B.L. Lucht, J. Electrochem. Soc. 152 (2005) A2327–A2334.
[13] E. Zinigrad, L. Larush-Asraf, J.S. Gnanaraj, M. Sprecher, D. Aurbach, Thermochim. Acta 438 (2005) 184–191.
[14] M. Broussely, P. Biensan, F. Bonhomme, P. Blanchard, S. Herreyre, K. Nechev, R.J. Staniewicz, J. Power Sources 146 (2005) 90–96.
[15] M. Broussely, S. Herreyre, P. Biensan, P. Kasztejna, K. Nechev, R.J. Staniewicz, J. Power Sources 97–98 (2001) 13–21.
[16] J. Vetter, P. Novák, M.R. Wagner, C. Veit, K.C. Möller, J.O. Besenhard, M. Winter, M. Wohlfahrt-Mehrens, C. Vogler, A. Hammouche, J. Power Sources 147 (2005) 269–281.
[17] Q. Wang, J. Sun, X. Yao, C. Chen, J. Electrochem. Soc. 153 (2006) A329–A333.
[18] J.-i. Yamaki, H. Takatsuji, T. Kawamura, M. Egashira, Solid State Ionics 148 (2002) 241–245.
[19] J. Jiang, J. Chen, J.R. Dahn, J. Electrochem. Soc. 151 (2004) A2082–A2087.
[20] J.R. Dahn, E.W. Fuller, M. Obrovac, U. von Sacken, Solid State Ionics 69 (1994) 265–270.
[21] P. Dan, E. Mengeritski, Y. Geronov, D. Aurbach, I. Weisman, J. Power Sources 54 (1995) 143–145.
[22] E. Peled, J. Electrochem. Soc. 126 (1979) 2047–2051.
[23] E. Peled, D. Golodnitsky, G. Ardel, V. Eshkenazy, Electrochim. Acta 40 (1995) 2197–2204.

[24] A. Killis, J.F. LeNest, A. Gandini, H. Cheradame, J. Polym. Sci. Polym. Phys. Ed. 19 (1981) 1073–1080.
[25] C.V. Nicholas, D.J. Wilson, C. Booth, J.R.M. Giles, Br. Polym. J. 20 (1988) 289–292.
[26] S. Sylla, J.Y. Sanchez, M. Armand, Electrochim. Acta 37 (1992) 1699–1701.
[27] T. Hamaide, A. Goux, M.-F. Llauro, R. Spitz, A. Guyot, Die Angew. Makromol. Chem. 237 (1996) 55–77.
[28] G. Goulart, S. Sylla, J.-Y. Sanchez, M. Armand, in: B. Scrosati (Ed.), Second Int. Symp. On Polymer Electrolytes, 1990, pp. 99–105. Amsterdam.
[29] G.B. Appetecchi, G. Dautzenberg, B. Scrosati, J. Electrochem. Soc. 143 (1996) 6–12.
[30] D. Fauteux, A. Massucco, M. McLin, M. Van Buren, J. Shi, Electrochim. Acta 40 (1995) 2185–2190.
[31] J.-H. Shin, W.A. Henderson, S. Passerini, J. Electrochem. Soc. 152 (2005) A978–A983.
[32] J.-H. Shin, W.A. Henderson, S. Passerini, Electrochem. Solid State Lett. 8 (2005) A125–A127.
[33] J.H. Shin, W.A. Henderson, G.B. Appetecchi, F. Alessandrini, S. Passerini, Electrochim. Acta 50 (2005) 3859–3865.
[34] J.-H. Shin, W.A. Henderson, S. Scaccia, P.P. Prosini, S. Passerini, J. Power Sources 156 (2006) 560–566.
[35] P.C. Howlett, D.R. MacFarlane, A.F. Hollenkamp, Electrochem. Solid State Lett. 7 (2004) A97–A101.
[36] E. Paillard, Q. Zhou, W.A. Henderson, G.B. Appetecchi, M. Montanino, S. Passerini, J. Electrochem. Soc. 156 (2009) A891–A895.
[37] M. Joost, G.T. Kim, M. Winter, S. Passerini, Electrochim. Acta 113 (2013) 181–185.
[38] G.T. Kim, G.B. Appetecchi, M. Carewska, M. Joost, A. Balducci, M. Winter, S. Passerini, J. Power Sources 195 (2010) 6130–6137.
[39] M. Joost, M. Kunze, S. Jeong, M. Schönhoff, M. Winter, S. Passerini, Electrochim. Acta 86 (2012) 330–338.
[40] G.B. Appetecchi, G.T. Kim, M. Montanino, F. Alessandrini, S. Passerini, J. Power Sources 196 (2011) 6703–6709.
[41] M. Wetjen, G.-T. Kim, M. Joost, M. Winter, S. Passerini, Electrochim. Acta 87 (2013) 779–787.
[42] M. Wetjen, G.-T. Kim, M. Joost, G.B. Appetecchi, M. Winter, S. Passerini, J. Power Sources 246 (2014) 846–857.
[43] Y. Xia, T. Fujieda, K. Tatsumi, P.P. Prosini, T. Sakai, J. Power Sources 92 (2001) 234–243.
[44] D.W. Murphy, P.A. Christian, F.J. DiSalvo, J.V. Waszczak, Inorg. Chem. 18 (1979) 2800–2803.
[45] M.S. Whittingham, J. Electrochem. Soc. 123 (1976) 315–320.
[46] C. Delmas, H. Cognac-Auradou, J.M. Cocciantelli, M. Ménétrier, J.P. Doumerc, Solid State Ionics 69 (1994) 257–264.
[47] C. Delmas, H. Cognac-Auradou, J. Power Sources 54 (1995) 406–410.
[48] G.B. Appetecchi, F. Alessandrini, M. Carewska, T. Caruso, P.P. Prosini, S. Scaccia, S. Passerini, J. Power Sources 97–98 (2001) 790–794.
[49] P.P. Prosini, S. Passerini, R. Vellone, W.H. Smyrl, J. Power Sources 75 (1998) 73–83.
[50] G.B. Appetecchi, J.H. Shin, F. Alessandrini, S. Passerini, J. Power Sources 143 (2005) 236–242.
[51] G.B. Appetecchi, M. Montanino, D. Zane, M. Carewska, F. Alessandrini, S. Passerini, Electrochim. Acta 54 (2009) 1325–1332.
[52] G.B. Appetecchi, S. Scaccia, C. Tizzani, F. Alessandrini, S. Passerini, J. Electrochem. Soc. 153 (2006) A1685–A1691.
[53] W.A. Henderson, S. Passerini, Chem. Mater. 16 (2004) 2881–2885.
[54] W. Qiu, M. Pyda, E. Nowak-Pyda, A. Habenschuss, B. Wunderlich, Macromolecules 38 (2005) 8454–8467.